Published online January 18, 2018

Original Research

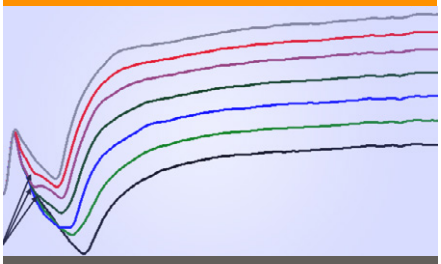

Interpreting TDR Signal Propagation through Soils with Distinct Layers of Nonaqueous-Phase Liquid and Water Content

A. Comegna,* A. Coppola, G. Dragonetti, G. Severino, and A. Sommella

Several studies have demonstrated that time-domain reflectometry (TDR) has an enormous potential to detect and monitor nonaqueous-phase liquids (NAPLs) in uniformly contaminated soils with reference to different-textured soils and under different saturation conditions. Few attempts have been proposed to describe NAPL distribution by using TDR when a contaminated front propagates through a soil. In this study, the TDR response in the presence of NAPL-contaminant transport processes was investigated in a homogeneous soil under confined conditions with a series of laboratory-controlled tests. The laboratory procedure involved measurements of dielectric permittivity (ε_b) and electrical conductivity (EC_b) and the acquisition of the reflected TDR waveforms. The experimental framework was designed to simulate sharp NAPL fronts that moved in the soil columns and generated zones of contrasting permittivity. During the experiments, different initial conditions were assumed, as well as different degrees of contamination, by varying the volumetric water (θ_w) and NAPL (θ_{NAPL}) contents. The acquired TDR waveforms were systematically analyzed to deduce the influence of NAPLs on TDR signal propagation. A general procedure to determine the location of an NAPL-contaminated front within a soil column was developed. Equipment calibration, measurement accuracy, and error sources were investigated in relation to the experimental procedure setup and the column preparation conditions. The results show that there may be some difficulties when interpreting TDR signals to locate the NAPL front for two main reasons: first, the expected additional reflection at the interface is not always distinguishable; second, there may be problems even locating both the first peak and the reflection point at the end of the TDR probe, especially when the signal shifts from a low to a high impedance layer. The suggested methodology provides a tool to overcome such intrinsic difficulties in NAPL front detection during the propagation of the contaminant.

Core Ideas

- The TDR response in the presence of NAPL transport was investigated in a homogeneous soil.
- The experimental framework was designed to simulate sharp NAPL fronts that moved in the soil.
- The TDR waveforms were analyzed to deduce the influence of NAPLs on TDR signal propagation.
- A general procedure to determine the location of an NAPL-contaminated front was developed.

A. Comegna and A. Coppola, School of Agricultural, Forestry, Food and Environmental Sciences (SAFE), Univ. of Basilicata, Potenza 85100, Italy; G. Dragonetti, Mediterranean Agronomic Institute, Land and Water Division, IAMB, Bari 70010, Italy; G. Severino and A. Sommella, Dep. of Agricultural Sciences, Univ. of Naples "Federico II", 80138 Naples, Italy. *Corresponding author (alessandro.comegna@unibas.it).

Received 20 July 2017.
Accepted 20 Dec. 2017.
Supplemental material online.

Citation: Comegna, A., A. Coppola, G. Dragonetti, G. Severino, and A. Sommella. 2017. Interpreting TDR signal propagation through soils with distinct layers of nonaqueous-phase liquid and water content. Vadose Zone J. 16(13). doi:10.2136/vzj2017.07.0141

Vol. 16, Iss. 13, 2017
© Soil Science Society of America
5585 Guilford Rd., Madison, WI 53711 USA.
All rights reserved.

Abbreviations: DL, dry layer; EC, electrical conductivity; NAPL, nonaqueous-phase liquid; NCSL, nonaqueous-phase liquid contaminated soil layer; NWCSL, nonaqueous-phase liquid and water contaminated soil layer; TDR, time-domain reflectometry; W1L, soil–water mixture with a volumetric water content of 0.20; W2L, soil–water mixture with a volumetric water content of 0.30.

The widespread production and use of liquid petroleum products have provided ample opportunity for subsurface contamination from leaking underground storage tanks, pipelines, ruptures, and illegal disposal of waste materials, hazardous waste sites, and surface spills. The aqueous solubility of these organic liquid contaminants is low enough for them to exist in the subsurface as nonaqueous-phase liquids (NAPLs) but high enough to seriously degrade water quality (Geller and Hunt, 1993).

Remediation of NAPL sites requires accurate knowledge of the contaminant distribution in the soil profile and groundwater. Methods commonly used to characterize contaminated sites involve soil drilling, sampling, and the installation of monitoring wells for the collection of soil and water samples (Mercer and Cohen, 1990).

Given the cost of these technologies, other noninvasive techniques that belong to geophysical methods have been sought to characterize contaminated sites extensively. In particular, the time-domain reflectometry (TDR) technique has been proposed as potentially exhibiting sufficient sensitivity and lateral and vertical resolution for characterization of soil NAPL volumes (Persson and Berndtsson, 2002; Francisca and Montoro, 2012, Comegna et al., 2013, 2016).

During the past four decades, TDR has become a very important tool for laboratory and field measurement of soil water content (θ_w) and soil solution electrical conductivity (EC_w) in uniformly wetted profiles (Topp et al., 1980; Dalton et al., 1984; Rhoades et al., 1989). Topp et al. (1982) were the first to carry out a series of laboratory experiments on soil profiles to evaluate TDR response during the progression of a steep wetting front. They demonstrated both theoretically and experimentally that the TDR technique may be able to detect the interface of a front during an infiltration process, and they developed a two-layer model based on summing the travel times of the TDR waveforms in the layers. Based on these pioneering results, more recent experiments of a similar nature were subsequently developed by, among others, Nadler et al. (1991), Dasberg and Hopmans (1992), Feng et al. (1999), and Yu and Yu (2006).

The potential of the TDR technique in estimating NAPL presence in saturated and unsaturated soils, under the general hypothesis that NAPL and water are uniformly distributed in the soil sample, has also been extensively explored (Redman and DeRyck, 1994; Chenaf and Amara, 2001; Persson and Berndtsson, 2002; Haridy et al., 2004; Mohamed and Said, 2005; Moroizumi and Sasaki, 2006; Rinaldi and Francisca, 2006; Francisca and Montoro, 2012; Comegna et al., 2013, 2016).

The issue of characterizing the dielectric effect of an NAPL-contaminated plume that moves in the soil matrix is a further complication that has to date attracted little attention (e.g., Barnett, 2002; Yu and Yu, 2006; Zhan et al., 2013). However, a well organized, detailed experiment was conducted by Zhan et al. (2013). Using the TDR technique, they measured the bulk dielectric permittivity (ε_b) and the bulk electrical conductivity (EC_b) of a diesel-contaminated layer sandwiched in sand. During the experiment, they analyzed the reflected TDR signals, looking for singularities in the waveforms at the layer interface. According to the experimental results obtained, they concluded that their methodology may facilitate NAPL detection in a contaminated site when NAPL exists in a saturated or an unsaturated sand but not in the case of the contaminant distributed in a dry sand.

There is thus a need for further experiments to support the application of the TDR technique to describe soil dielectric behavior in the presence of an NAPL moving front. In this study, starting from the research of Zhan et al. (2013), we performed a series of laboratory NAPL-contaminant transport experiments in which we simulated different scenarios of practical interest, aiming to analyze the effects of a steep front on the shape of a TDR waveform. Finally, on the basis of the experimental results obtained, we developed a general methodology for evaluating the location in the soil profile of the NAPL front.

Theory

Theoretical Background and Operational Principles of TDR

The TDR technique is a well-established geophysical method to measure the dielectric permittivity of liquids and solids, described by a complex number ε_r^* (Robinson and Friedman, 2002):

$$\varepsilon_r^* = \varepsilon_r' - J\left[\varepsilon_r'' + \frac{\sigma}{\omega\varepsilon_0}\right] \quad [1]$$

where ε_r' is the real part of the dielectric permittivity, which accounts for the energy stored in the dielectrics at a given frequency and temperature, ε_r'' is the imaginary part due to relaxations, σ is the zero-frequency conductivity, ω is the angle frequency, $J = \sqrt{-1}$ is the imaginary number, and ε_0 is the permittivity in free space.

At the highest effective frequency of the TDR cable tester (200 MHz–1.5 GHz) where the dielectric losses can be assumed to be negligible, using a waveguide (or probe) of known length L, the bulk dielectric permittivity ε_b ($\cong$ the real part of permittivity) is measured from the propagation velocity v ($= 2L/t$) of an electromagnetic wave along the waveguide through the soil by

$$\varepsilon_b = \left(\frac{c}{v}\right)^2 \quad [2]$$

where c ($= 3 \times 10^8$ m s^{-1}) is the velocity of an electromagnetic wave in a vacuum (Topp et al., 1980) and t is the travel time, which represents the time that is needed by the TDR signal to travel back and forth to the waveguide of length L (m) and can be written as

$$t = \frac{2L}{c}\sqrt{\varepsilon_b} \quad [3]$$

which yields the direct dependence between the travel time t of the signal and the soil dielectric properties (i.e., ε_b).

Other important information that can be obtained from a TDR signal is the bulk electrical conductivity, EC_b, related to the magnitude of energy attenuation, which can be calculated using the method of Giese and Tiemann (1975):

$$EC_b = \frac{\varepsilon_0 c}{L}\frac{Z_0}{Z_c}\left(\frac{2V_0}{V_f} - 1\right) \quad [4]$$

where Z_0 is the characteristic probe impedance, Z_c is the TDR cable tester output impedance, V_0 is the incident pulse voltage (i.e., source voltage), and V_f is the return pulse voltage after multiple reflections have died out (i.e., long-term voltage). The value of EC_b depends on soil water content, electrical conductivity of the pore solution, tortuosity of the soil–pore system, and other factors related to the solid phase such as bulk density, clay content, and mineralogy.

Nonaqueous-Phase Liquid Front Detection in a Soil Profile

Here we analyze the possibility of identifying the location of an advancing steep NAPL front in a soil profile under the hypothesis that the soil is homogeneous from a textural point of view. Several researchers (Topp et al., 1982; Yu and Yu, 2006; Zhan et al., 2013; among others) have observed that when in a soil profile an impedance change occurs, this change may cause a distinguishable reflection on the TDR signal. This is due to the superposition of the incident and the reflected waves that generate either an in-phase or an out-of-phase signal, depending on the dielectric properties before and after the discontinuity (Mohamed, 2006).

If a wetting front containing water proceeds in a soil profile, it certainly produces a dielectric discontinuity along the transmission line. If this discontinuity at the interface is clear along the acquired TDR signal, the thickness of the front can be determined by the procedure of Topp et al. (1982), who suggested a way to calculate the front position in a soil profile in the presence of a sharp wetting front. According to this approach, in a porous medium with two layers, i and j, each with its own dielectric permittivity, ε_{bi} and ε_{bj}, and wave travel time, t_i and t_j, the partial length, L_i, of the transmission line in the ith layer can be estimated as

$$L_i = \frac{ct_i}{\sqrt{\varepsilon_{bi}}} \quad [5]$$

and the complementary length, L_j, in the jth layer may be determined as

$$L_j = L - L_i \quad [6]$$

where L is the total length of the transmission line (probe length).

In the presence of an NAPL-contaminating front, Zhan et al. (2013) demonstrated that in some circumstances (e.g., an NAPL layer sandwiched between two dry sand layers) the dielectric discontinuity across the two contrasting zones might not induce an appreciable variation in the reflection amplitude of the TDR signal, and thus Topp's approach becomes impossible to apply. To fill this gap and with the aim of exploring different possible scenarios of practical interest from those investigated by Zhan et al. (2013), we propose a methodology based on TDR waveform analysis, coupled with bulk soil electrical conductivity (EC_b) measurements. Electrical conductivity was selected as a candidate dielectric parameter for our approach because it is easy to determine (see, for example, Giese and Tiemann [1975] and Heimovaara et al. [1995]) once a long-term TDR signal has been acquired. Specifically, by using the TDR technique, the EC_b of the total volume sampled by the TDR probe can be utilized for calculating the thickness of the contaminated layer (L_{NWCSL}, where NWCSL is the NAPL + water contaminated soil layer) as a linear function of the EC_b:

$$L_{NWCSL} = aEC_b + b \quad [7]$$

where a and b are coefficients that have to be experimentally determined. Below we will show that the slope coefficient a and the intercept b of Eq. [7] mainly depend on the volumetric content of NAPL (θ_{NAPL}) and water (θ_w).

Materials and Methods

The Soil

The soil investigated in this study was a loam Eutric Cambisol (IUSS Working Group WRB, 2006) located in southern Italy. The soil texture was determined using hydrometer and sieving analysis (Day, 1965); soil organic C content was analyzed according to the Walkley–Black method as described by Allison (1965); the soil solution electrical conductivity (EC_w) was measured with the method proposed by Miller and Curtin (2007), while the soil pH was determined using a 1:1 soil/water ratio (Eckert, 1988). The Ap horizon of the Eutric Cambisol under study to a depth of 20 cm was classified as loam, with 41.4% sand, 16.4% clay, and 42.2% silt. It had porosity of 0.52%, organic C content of 0.30%, EC_w of 0.13 dS m^{-1}, and a pH of 8.40.

The NAPL used for the experiments was corn oil (ε_{NAPL} = 3.2; EC_{NAPL} = 0.055 dS m^{-1} at 25°C) with a density of 0.905 g cm^{-1} (at 25°C). The electrical conductivity of water used was 0.0005 dS m^{-1}.

Experimental Setup

The experimental apparatus consisted of a TDR unit (Tektronix 1502C cable tester) and a three-wire TDR probe, with waveguides 14.5 cm long and a coaxial cable 2 m long. The reflected signals were collected by a PC-based data acquisition-processing system. A MATLAB code based on the method of Baker and Allmaras (1990) was specifically developed for post-processing the acquired TDR signals to calculate the dielectric constant of each layer in the medium. Figure 1 gives a picture of the dielectric measurement system used in the experiments.

Experimental Design

A laboratory experiment was performed on repacked soil samples collected from the Ap horizon of the Eutric Cambisol. The experiment involved measurements of ε_b and EC_b conducted on a series of NAPL-contaminated samples. The experimental framework was designed to obtain soil cores with two distinct dielectric layers. One of the two layers was designed to have a certain volume of

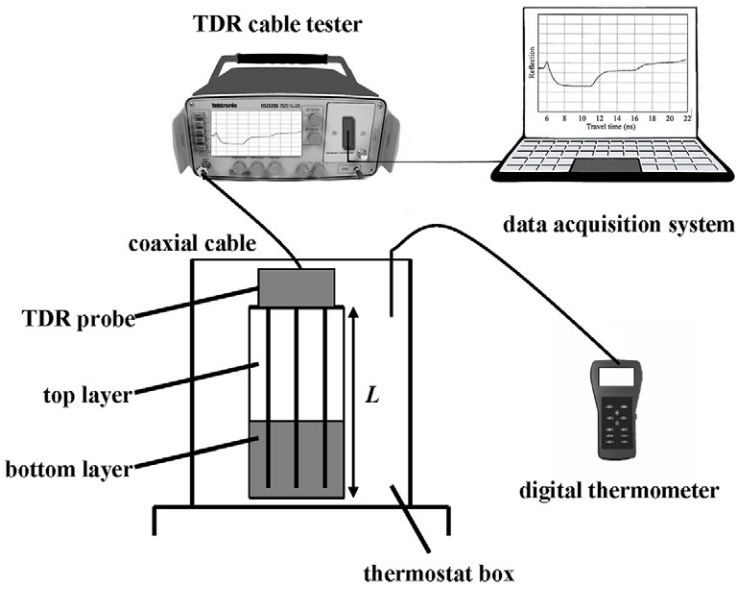

Fig. 1. Experimental setup used in the laboratory experiment, where L is the length of the entire soil column.

NAPL and water (NWCSL), whereas the complementary layer was either completely dry (dry layer, DL) or it was prepared with a fixed water content (water layers, W1L and W2L) or NAPL content (NAPL contaminated soil layer, NCSL). Further, in the procedure adopted, for the NWCSL, a known volumetric water content (θ_w) and volumetric NAPL content (θ_{NAPL}) were mixed together to obtain a certain volumetric fluid content θ_f (= $\theta_{NAPL} + \theta_w$). For a full factorial analysis, θ_f and the relative volume of NAPL in water ($\beta = \theta_{NAPL}/\theta_f$) were varied from 0.165 to 0.400 and from 0.10 to 0.75, respectively, with the purpose of achieving, at selected dielectric permittivity values (ε_b = 6, 9, and 12), different levels of soil contamination (for more details, see Comegna et al., 2016). The W1L and W2L layers are soil–water mixtures with known different θ_w of 0.20 and 0.30, respectively. Finally, the NCSL layer was prepared with the same volumetric NAPL content (θ_{NAPL}) as the NWCSL layer but with θ_w set to 0. In accordance with the procedure adopted, the thickness of the front was varied from 0 to 15 cm by 2.5-cm increments. In summary, we built soil cores with a homogeneous texture in which, due to the different mixtures of the two layers, we created "vertical fluid heterogeneity" in such a manner that it influenced the final shape of the TDR signal.

During the laboratory experiments, the dielectric response of the contaminated soil samples was studied with reference to four scenarios (1, 2, 3, and 4), in which, following the scheme in Fig. 2, the different layers were combined with each other by varying their thickness. For each scenario, we considered seven different steps.

In Scenario 1, we simulated a soil sample that was at the beginning completely dry (DL) or at a uniform water content (W1L or W2L). At a certain time, we assumed that the contaminant source was applied at the sample bottom, such that the front moved upward, reaching in sequence the tip and the top of the TDR waveguide. In Scenario 2, the initial condition was similar to that of Scenario 1, but now we hypothesized that the NAPL leaked from the top of the soil sample such that the contaminant source propagated downward. In the last two scenarios (3 and 4), at the beginning soil samples were originally NAPL contaminated. We then simulated the water fraction gradually leaving the soil sample from the bottom (Scenario 3) and from the top (Scenario 4) of the soil profile. For each step of the experimental framework, we acquired measurements of both ε_b and EC_b, and we recorded the TDR waveforms for further investigations.

Sampling Properties and Testing Procedures

During the laboratory experiment, the soil samples were oven dried at 105°C and sieved at 2 mm. To perform the designed experiment, different soil mixtures were prepared as presented in Table 1.

All soil samples (except the case of dry soil samples) were mixed together, shaken, and then kept for 24 h in sealed plastic bags to avoid any evaporation. During this time, to guarantee a uniform distribution and adsorption of fluids by the soil matrix, the soil mixture was stirred frequently (Persson and Berndtsson, 2002; Comegna et al., 2016).

After this step, the soil was then immediately placed in cylindrical polyvinyl chloride containers (15 cm high and 9.5 cm in diameter) in several steps, during which it was carefully compacted until a 1.27 g cm^{-3} bulk density was attained. Soil samples were kept at a fairly constant temperature of 25°C during the TDR measurements using a thermostat box.

For preparing the stratified samples, we adopted the procedure suggested by Yu and Yu (2006), in which a thin layer of plastic film was placed on the surface separating the two layers. A hole with a slightly larger diameter than that of the external separation distance between the TDR rods was made in the center of the plastic film to prevent the rods from penetrating and distorting the plastic film. After the separation film was in place, another layer of soil was compacted on top of the bottom layer. For preparing a soil sample at a desired bulk density, a premeasured weight of soil was placed in the cylinder and pressed until it filled the desired layer thickness and thus was compacted to the desired porosity. This process was repeated for all the soil samples used in the experiment. Before starting the experiments, several tests were performed to validate the procedure adopted. Finally, after packing, a TDR probe was inserted vertically into the top layer of each soil sample. To avoid any difference in TDR readings (which may be generated by dissimilar geometric characteristics of the probe), all the measurements were made with the same TDR probe (see Comegna et al., 2016). Overall, there were 504 NAPL-contaminated soil

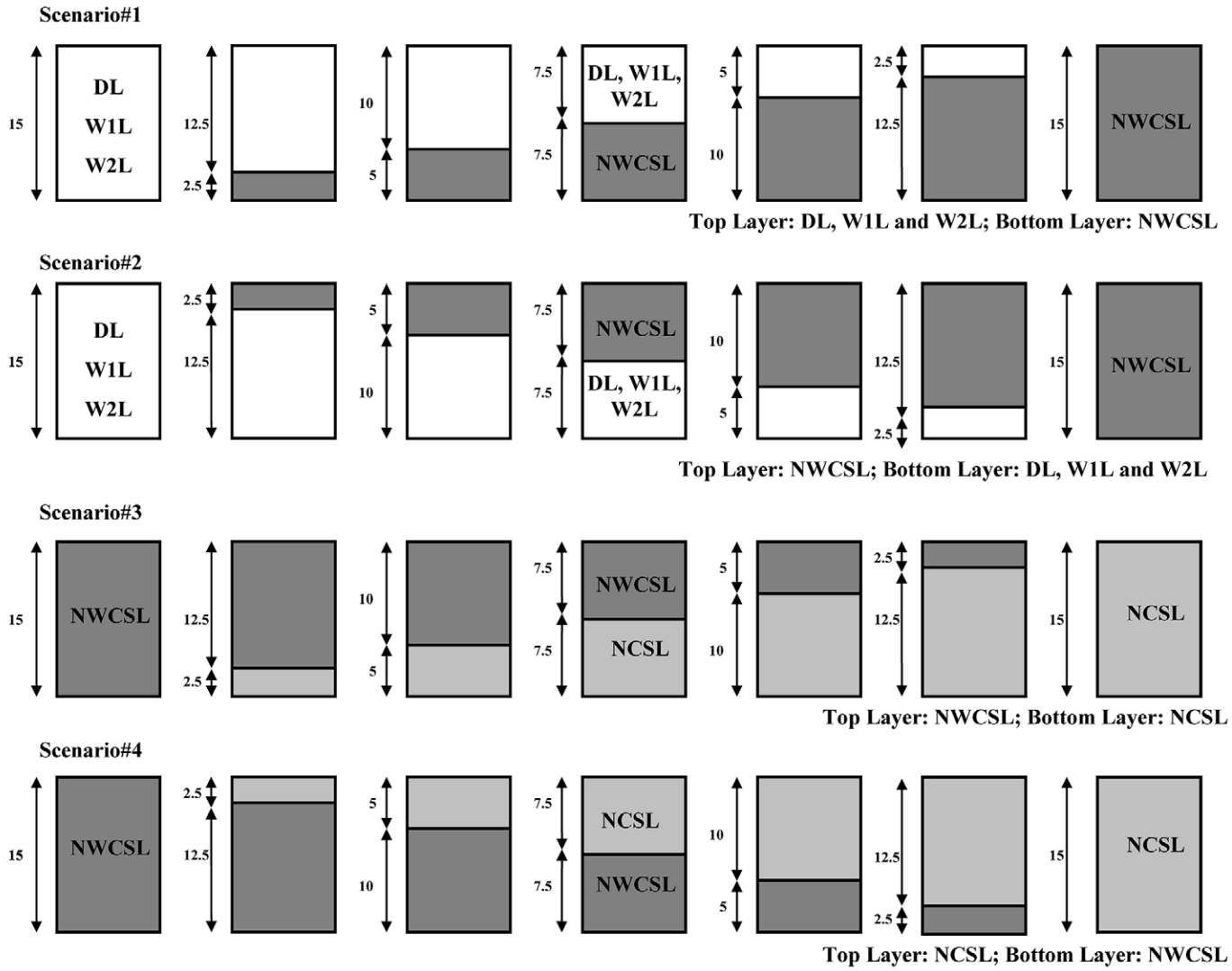

NWCSL, NAPL+water contaminated soil layer; NCSL, NAPL contaminated soil layer; W1L, soil–water layer with volumetric water content of 0.20; W2L, soil–water layer with volumetric water content of 0.30; DL, dry layer.

Fig. 2. Experimental schemes and the thickness of the incoming contaminated layer for the four scenarios prepared (units in centimeters).

Table 1. Combinations of NAPL volume (V_{NAPL}) and moisture volume (V_w) for the different soil mixtures for determined levels of contamination (β) at different total fluid volumes (θ_f).

		NAPL + water contaminated soil layer			NAPL contaminated soil layer		Soil–water layer 1		Soil–water layer 2		Dry soil layer	
ε_b†	β	θ_f	V_{NAPL}	V_w	θ_f	V_{NAPL}	θ_f	V_w	θ_f	V_w	θ_f	V_f
			—— cm^3 ——			cm^3		cm^3		cm^3		cm^3
6	0.25	0.165	44	132	0.041	44	0.200	213	0.300	319	0	0
6	0.50	0.230	122	122	0.115	122	0.200	213	0.300	319	0	0
6	0.75	0.390	311	104	0.293	311	0.200	213	0.300	319	0	0
9	0.20	0.240	51	204	0.048	51	0.200	213	0.300	319	0	0
9	0.40	0.310	132	198	0.124	132	0.200	213	0.300	319	0	0
9	0.60	0.430	274	183	0.258	274	0.200	213	0.300	319	0	0
12	0.10	0.280	30	268	0.028	30	0.200	213	0.300	319	0	0
12	0.30	0.350	112	260	0.105	112	0.200	213	0.300	319	0	0
12	0.40	0.400	170	255	0.160	170	0.200	213	0.300	319	0	0

† The expected dielectric permittivity (ε_b) values refer to a contaminated layer 15 cm high.

samples (189 measurements are available for Scenario 1, 189 measurements for Scenario 2, 63 measurements for Scenario 3, and 63 measurements for Scenario 4) used for a full factorial analysis. Furthermore, for each scenario, an independent validation dataset (consisting of 90 contaminated soil samples for Scenarios 1 and 2 and 25 contaminated soil samples for Scenarios 3 and 4) was prepared for testing the procedure developed. In each mixture of soil, water, and oil, 10 TDR measurements were taken and averaged immediately after packing.

Statistical Indices for Model Performance Evaluation

The performance of Eq. [5] and [7] was quantified by using two different criteria: (i) relative error (E_{rel}), which defines the difference between the ith true value in the observed dataset and the corresponding estimated value in a modeled dataset with respect to the true value; and (ii) maximum absolute error (ME), which is the maximum absolute difference observed between measured and expected values. These indices were computed according to the following relations (Legates and McCabe, 1999; International Union of Pure and Applied Chemistry, 1997; Reusser et al., 2009):

$$E_{rel} = \frac{O_i - E_i}{O_i} \quad [8]$$

$$ME = \max_{i=1...n} |O_i - E_i| \quad [9]$$

where E_i is the prediction (model-simulated data), O_i is the true value (observed data), and n is the number of observations.

Results and Discussion

Influence of a Nonaqueous-Phase Liquid Front on TDR Signal Shape in Soil Profiles

A selection of the acquired TDR signals, under the different experimental scenarios illustrated above, are shown in Fig. 3 (each soil sample is identified by the soil layer: NWCSL, NCSL, W1L, W2L, or DL, followed by a number that indicates the thickness of the layer; the first label refers to the top layer, whereas the second label refers to the bottom layer). Reflections across the interfaces of the different layers can be detected in some cases. Figure 3a (Scenario 1) and Fig. 3b (Scenario 3) present similar trends: as the thickness of the top layer decreases, the first peak location appears (virtually) to shift to the right and tends to decrease pronouncedly when approaching the final condition (i.e., DL or NCSL). Figures 3c and 3d show the W1L–NWCSL and NWCSL–W1L TDR signal sequences (Scenarios 1 and 2, respectively). In these cases, the reflections at the interfaces are not clear even by zooming between the first peak and the reflection at the end of the probe. The absence of an evident additional reflection at the layer interface is probably due to the superposition effect of the incident and the reflected signals that produces, in these two cases, a relatively flat waveform without a significant variation in the reflection coefficient magnitude (Yu and Yu, 2006; Mohamed, 2006).

On the contrary, Fig. 3e and 3f show that, with reference to the same scenario conditions in Fig. 3c and 3d but increasing the amount of water in the uncontaminated layer, the reflection of the transmitted pulse at the interface becomes clear, especially in the W2L2.5–NWCSL12.5, W2L5–NWCSL10, and W2L7.5–NWCSL7.5 cases of Scenario 1, where the transition between layers is noted by a backward position of the reflection (Yu and Yu, 2006). In Fig. 3f, for the sake of clarity, we illustrate only NWCSL–W2L interfaces at 5 and 10 cm (i.e., NWCSL5–W2L10 and NWCSL10–W2L5), as well as the initial (W2L) and final (NWCSL) soil conditions. In the latter case, during the transition from the low-permittivity layer to the high-permittivity layer, the position of the reflection moves backward, with a downward concavity. Finally, Fig. 3g and 3h (Scenarios 2 and 4) show a reduction in the travel time t as the thickness of the top layer increases. In some cases (see the blue arrows), in accordance with Zhan et al. (2013), the additional reflection point of the transmitted pulse due to the layer presence is visible. No more significant indication may be inferred from the whole acquired TDR waveforms dataset.

In summary, in all the illustrated scenarios we often noted: (i) that the position of the interface could not be easily detected from the TDR signal; or (ii) that the interface was even completely absent. These observations definitively clarify that the difficulty in the dielectric permittivity calculation, which is necessary for implementing Topp's approach (Eq. [5]), limits the possibility of fully monitoring the displacement of NAPLs in soils. On the other hand, the electrical conductivity of the contaminated system can always be computed if the TDR signal is acquired in a proper observation window. Moreover, EC_b showed a linear dependence (most of the computed R^2 are >0.90) on the thickness of the contaminated layer (L_{NWCSL}), which is a fundamental point in the present research. This dependence allowed us to develop Eq. [7], which does not need to locate a visible interface in contaminated soil profiles, as shown below.

Contaminated Front Detection

The complete dataset of computed a and b coefficients of Eq. [7] is summarized in Table 2, where it is separated by scenario and level of NAPL contamination. Table 2 contains data from Scenarios 1 and 2 (in which wetting NAPL fronts that moved upward and downward, respectively, in the soil sample were simulated) and data from Scenarios 3 and 4 (in which the NAPL-contaminated soil leaked water from the top or the bottom of the contaminated soil profile). For each scenario and degree of NAPL contamination (β), nine pairs of a and b coefficients were determined. Once coefficients a and b for a selected scenario are available, Eq. [7] may be implemented for continuously monitoring the position of the contaminated interface by just measuring EC_b.

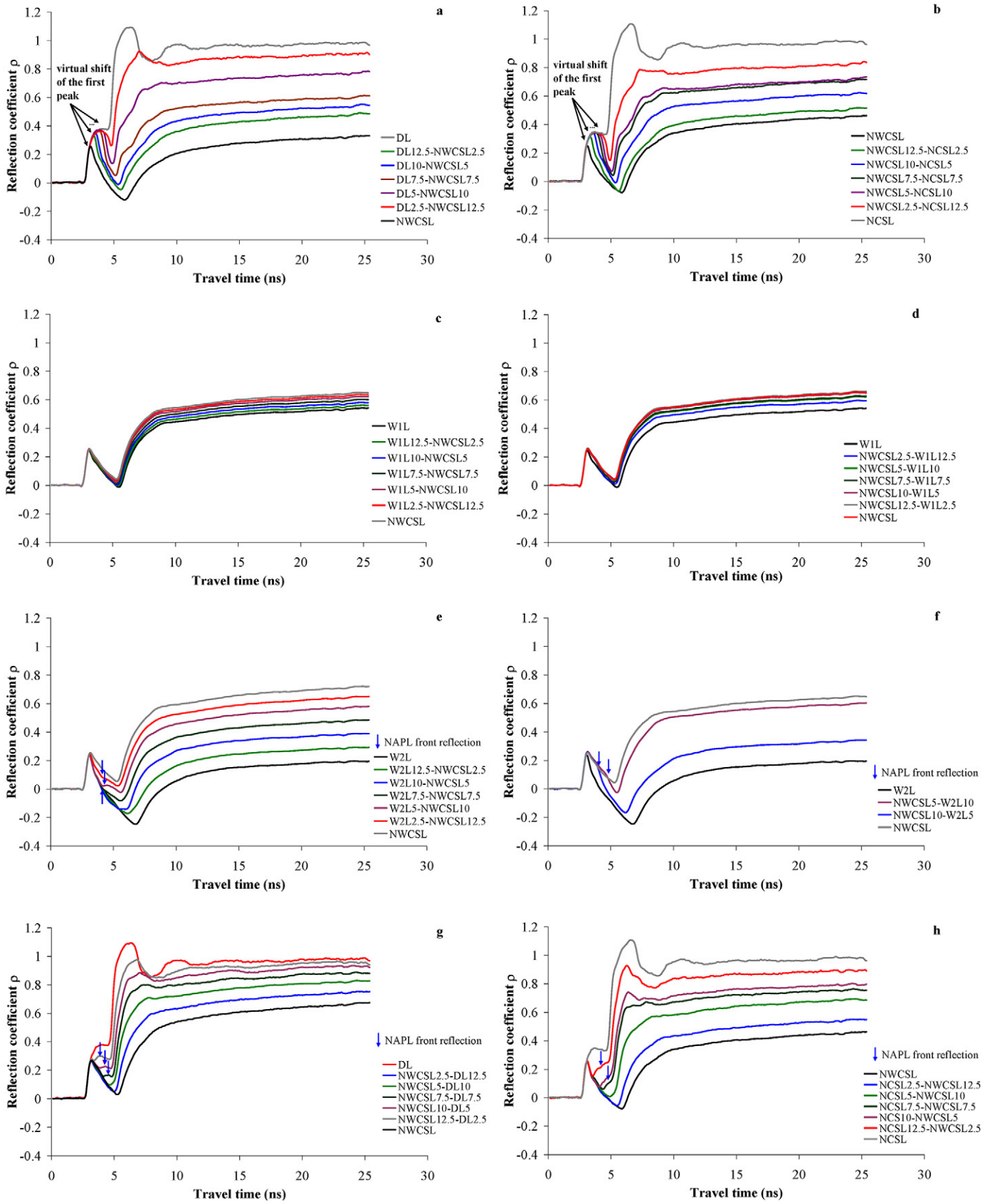

Fig. 3. Selected reflection waveforms of contaminated soil samples for the different designed scenarios (NWCSL, nonaqueous-phase liquid [NAPL] + water contaminated soil layer; NCSL, NAPL contaminated soil layer; W1L, soil–water layer with volumetric water content of 0.20; W2L, soil–water layer with volumetric water content of 0.30; DL, dry layer).

Table 2. Estimated coefficients *a* and *b* of Eq. [7] for the four scenarios and for assigned bulk dielectric conductivity (ε_b) and relative volume of nonaqueous-phase liquid (NAPL) in water (β) values. Five tests were run for each fitted *a* and *b* coefficient.

Layer ID†					
Top layer	Bottom layer	ε_b	β	*a*	*b*
		Scenario 1			
DL	NWCSL	6	0.25	−129.29	13.09
DL	NWCSL	6	0.50	−125.73	12.88
DL	NWCSL	6	0.75	−104.12	13.35
DL	NWCSL	9	0.20	−126.74	21.16
DL	NWCSL	9	0.40	−49.23	14.11
DL	NWCSL	9	0.60	−65.66	15.61
DL	NWCSL	12	0.10	−54.15	17.72
DL	NWCSL	12	0.30	−59.35	17.67
DL	NWCSL	12	0.40	−61.98	19.97
W1L	NWCSL	6	0.25	98.31	−7.36
W1L	NWCSL	6	0.50	84.99	−5.68
W1L	NWCSL	6	0.75	81.21	−1.198
W1L	NWCSL	9	0.20	89.20	−11.13
W1L	NWCSL	9	0.40	94.946	−14.07
W1L	NWCSL	9	0.60	104.01	−13.68
W1L	NWCSL	12	0.10	97.34	−22.74
W1L	NWCSL	12	0.30	91.01	−21.49
W1L	NWCSL	12	0.40	87.97	−21.82
W2L	NWCSL	6	0.25	62.96	−5.83
W2L	NWCSL	6	0.50	38.97	−2.11
W2L	NWCSL	6	0.75	46.94	−3.13
W2L	NWCSL	9	0.20	35.94	−1.92
W2L	NWCSL	9	0.40	48.72	−6.87
W2L	NWCSL	9	0.60	63.11	−12.33
W2L	NWCSL	12	0.10	281.82	−99.84
W2L	NWCSL	12	0.30	68.39	−20.40
W2L	NWCSL	12	0.40	131.59	−44.31
		Scenario 2			
NWCSL	DL	6	0.25	−135.24	12.66
NWCSL	DL	6	0.50	−129.76	12.84
NWCSL	DL	6	0.75	−181.95	14.40
NWCSL	DL	9	0.20	−95.72	14.23
NWCSL	DL	9	0.40	−42.65	12.22
NWCSL	DL	9	0.60	−65.48	13.94
NWCSL	DL	12	0.10	−70.24	17.71
NWCSL	DL	12	0.30	−44.35	13.54
NWCSL	DL	12	0.40	−62.69	18.10
NWCSL	W1L	6	0.25	91.40	−4.51
NWCSL	W1L	6	0.50	77.21	−3.32
NWCSL	W1L	6	0.75	90.36	−1.67
NWCSL	W1L	9	0.20	77.16	−7.02
NWCSL	W1L	9	0.40	103.13	−13.17
NWCSL	W1L	9	0.60	103.8	−12.04
NWCSL	W1L	12	0.10	78.23	−16.82
NWCSL	W1L	12	0.30	94.88	−18.21
NWCSL	W1L	12	0.40	85.26	−17.74
NWCSL	W2L	6	0.25	102.18	−13.52
NWCSL	W2L	6	0.50	35.79	−1.42
NWCSL	W2L	6	0.75	43.58	−2.47
NWCSL	W2L	9	0.20	50.76	−4.54
NWCSL	W2L	9	0.40	50.59	−5.47
NWCSL	W2L	9	0.60	51.01	−7.15
NWCSL	W2L	12	0.10	102.8	−30.66
NWCSL	W2L	12	0.30	70.31	19.60
NWCSL	W2L	12	0.40	85.13	−24.77
		Scenario 3			
NWCSL	NCSL	6	0.25	−182.96	17.42
NWCSL	NCSL	6	0.50	−129.76	12.84
NWCSL	NCSL	6	0.75	−166.43	16.17
NWCSL	NCSL	9	0.20	−106.9	19.52
NWCSL	NCSL	9	0.40	−96.16	20.89
NWCSL	NCSL	9	0.60	−153.87	25.74
NWCSL	NCSL	12	0.10	−54.97	18.75
NWCSL	NCSL	12	0.30	−43.74	15.55
NWCSL	NCSL	12	0.40	−58.35	18.58
		Scenario 4			
NCSL	NWCSL	6	0.25	−162.44	12.37
NCSL	NWCSL	6	0.50	19.58	13.25
NCSL	NWCSL	6	0.75	−232.66	17.61
NCSL	NWCSL	9	0.20	−86.73	16.64
NCSL	NWCSL	9	0.40	−111.77	19.89
NCSL	NWCSL	9	0.60	−72.38	19.95
NCSL	NWCSL	12	0.10	−51.04	16.14
NCSL	NWCSL	12	0.30	−50.39	13.21
NCSL	NWCSL	12	0.40	63.80	17.77

† DL, dry layer; NWCSL, NAPL + water contaminated soil layer; W1L, soil–water layer with volumetric water content of 0.20; W2L, soil–water layer with volumetric water content of 0.30; NCSL, NAPL-contaminated soil layer.

The results presented suggest that, for each scenario, coefficients *a* and *b* vary with the amount of NAPL and water (if present) within the soil specimen. Moreover, this variation generates, in the Cartesian plane, L_{NWCSL}–EC_b correlations that can be positive or negative, according to the specific scenario investigated.

A selection of the experimental L_{NWCSL}–EC_b relationships (validation dataset) and the corresponding computed linear regressions are shown in Fig. 4 for each scenario. The figure clearly demonstrates that the thickness of the contaminated layer is linearly correlated, as indicated by the R^2 values, with the electrical conductivity of the contaminated medium.

The L_{NWCSL} computed from Eq. [5] and [7], respectively, and the known L_{NWCSL} content are illustrated in Fig. 5. Only 44 of the 504 measurements obtained from the laboratory experiment are shown. The selected TDR signals are those in which the contaminated front

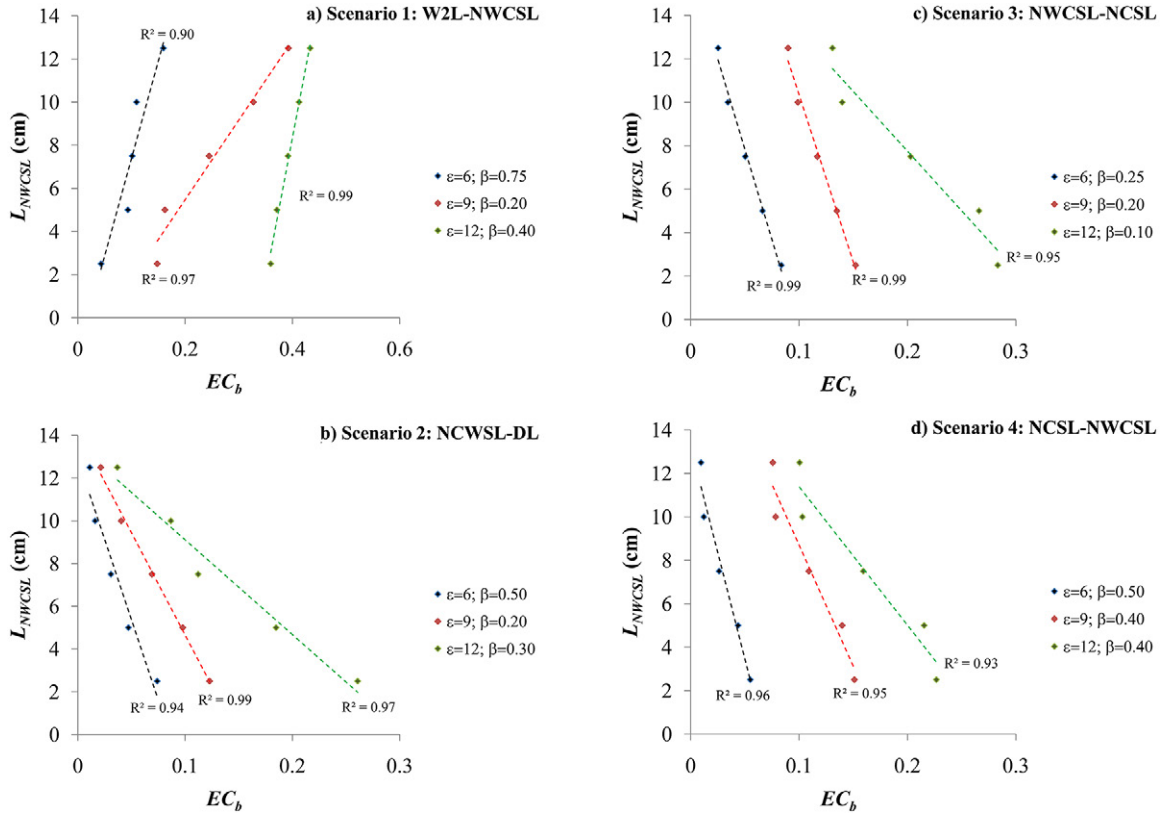

Fig. 4. Selection of experimental relationships between the measured thickness of the NAPL + water contaminated soil layer (L_{NWCSL}) and electrical conductivity (EC_b) under different bulk dielectric permittivities (ε) and relative volumes of nonaqueous-phase liquid (NAPL) in water (β) for (a) Scenario 1 with a soil–water layer with a volumetric water content of 0.30 overlying an NWCSL, (b) Scenario 2 with an NWCSL overlying a dry layer (DL), (c) Scenario 3 with an NWCSL overlying an NAPL-contaminated soil layer (NCSL), and (d) Scenario 4, with an NCSL overlying an NWCSL.

was observable. Thus a direct comparison between Eq. [5] and [7] was made possible. For the sake of completeness, the results presented in Fig. 5 are illustrated in Supplemental Tables S1 and S2.

The relative error (E_{rel}) for the different scenarios and with reference to the 44 selected data was also calculated (Fig. 6). The computed statistical index shows the satisfactory agreement of predictions from Eq. [7] with the experimental data, which are better than those obtained by means of Eq. [5]. The E_{rel} varies between −0.74 and 1.17 (Eq. [5]) and −0.41 and 0.24 (Eq. [7]). The mean error calculated among the different scenarios ranges between 2.8 and 4 cm (Eq. [5]) and between 0.9 and 2.1 cm (Eq. [7]).

Considering the complexity of the investigated process, these results confirm the scientific consistency of the developed methodology and its general applicability to determining the presence and relative position of an NAPL front in real cases.

Conclusions

As discussed by Zhan et al. (2013), organic contaminants such as hydrocarbons may exist and may be distributed both in the unsaturated zone and in the groundwater. Nonaqueous-phase liquids penetrate the subsurface as an immiscible pure oil phase, which migrates in response to viscous, gravity, and capillary forces, which may cause the formation of immobile residuals or mobile pools.

With reference to the results illustrated above, we may conclude that the NAPL front in some cases can be directly localized due to a clearly visible additional reflection at the layer interface. This represents a desirable condition, which unfortunately cannot always be achieved nor is a priori predictable. The final shape of a TDR signal in the presence of an incoming front, as explained and shown, depends on the interplay of several factors that, combined with one another, may or may not evidence the reflection across the front. Thus an advance in this research field lies in the possibility of characterizing the front of a contaminant plume in situations in which the TDR waveform does not clearly show any apparent reflection at the interface, which at present remains a fundamental condition for identifying the moving front in a soil profile (Topp et al., 1982; Dasberg and Hopmans, 1992; Zhan et al., 2013).

For this reason, the present study aimed to develop a new methodological approach for electromagnetic characterization of NAPL-contaminated soil sites to overcome current difficulties. The study focused on the differences in electrical conductivity observable during the progression of the contaminant in the soil

profile. The model formulation (Eq. [7]) utilized the linear dependence between the electrical conductivity (EC_b) and the thickness of the contaminated layer (L_{NWCSL}), which were experimentally observed and described in this study.

The approach requires additional experiments and datasets for model calibration in different pedological contexts, mainly to confirm the potential of the methodology developed and to fully explore the physical basis of the observed relationship between L_{NWCSL} and EC_b. Full field-scale tests should also be conducted to evaluate the performance of Eq. [7] under real field conditions.

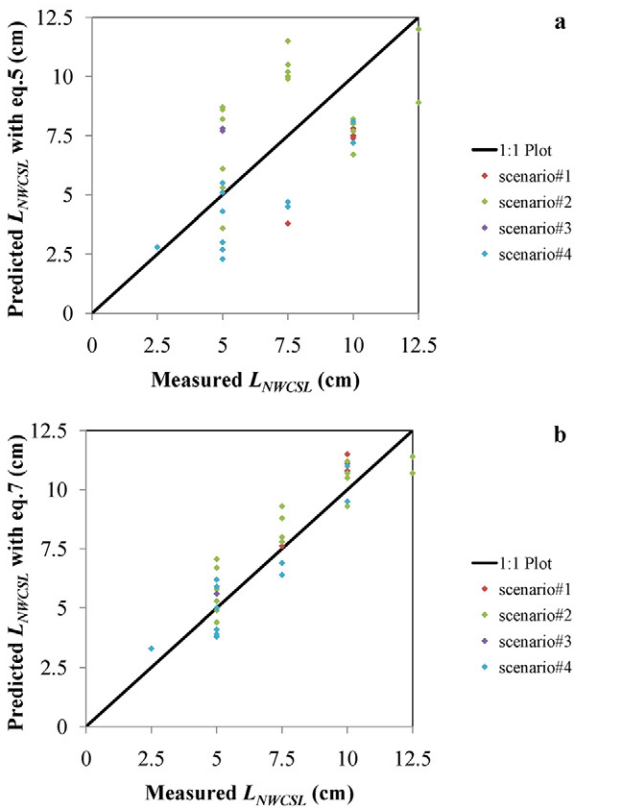

Fig. 5. The thickness of the NAPL-contaminated layer (L_{NWCSL}) as measured and predicted by (a) Eq. [5] and (b) Eq. [7] for the four scenarios investigated.

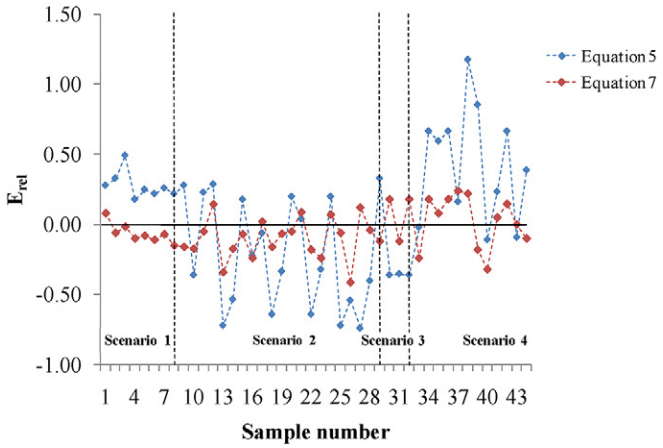

Fig. 6. Relative error (E_{rel}) of Eq. [5] and [7] computed for the four scenarios.

References

Allison, L.E. 1965. Organic carbon. In: C.A. Black et al., editors, Methods of soil analysis. Part 2. Agron. Monogr. 9. ASA, Madison, WI. p. 1367–1378. doi:10.2134/agronmonogr9.2.c39

Baker, J.M., and R.R. Allmaras. 1990. System for automating and multiplexing soil moisture measurement by time domain reflectometry. Soil Sci. Soc. Am. J. 54:1–6. doi:10.2136/sssaj1990.03615995005400010001x

Barnett, D.A. 2002. Detection of diesel fuel leakage from underground tank using time domain reflectometry. M.S. thesis. Northwest Missouri State Univ, Maryville.

Chenaf, D., and N. Amara. 2001. Time domain reflectometry for the characterization of diesel contaminated soils. In: C.H. Dowding et al., editors, Proceedings of the 2nd International Symposium and Workshop on Time Domain Reflectometry for Innovative Geotechnical Applications, Evanston, IL. 5–7 Sept. 2001. Infrastructure Technol. Inst., Northwestern Univ., Evanston, IL.

Comegna, A., A. Coppola, G. Dragonetti, and A. Sommella. 2013. Dielectric response of a variable saturated soil contaminated by non-aqueous phase liquids (NAPLs). Procedia Environ. Sci. 19:701–710. doi:10.1016/j.proenv.2013.06.079

Comegna, A., A. Coppola, G. Dragonetti, and A. Sommella. 2016. Estimating non-aqueous phase liquid (NAPL) content in variable saturated soils using time domain reflectometry (TDR). Vadose Zone J. 15(5). doi:10.2136/vzj2015.11.0145

Dalton, F.N., W.N. Herkelrath, D.S. Rawlins, and J.D. Rhoades. 1984. Time-domain reflectometry: Simultaneous measurement of soil water content and electrical conductivity with a single probe. Science 224:989–990. doi:10.1126/science.224.4652.989

Dasberg, S., and J.W. Hopmans. 1992. Time domain reflectometry calibration for uniformly and nonuniformly wetted sandy and clayey loam soils. Soil Sci. Soc. Am. J. 56:1341–1345. doi:10.2136/sssaj1992.03615995005600050002x

Day, P.R. 1965. Particle fractionation and particle-size analysis. In: C.A. Black et al., editors, Methods of soil analysis. Part 1. ASA, Madison, WI. p. 545–567. doi:10.2134/agronmonogr9.1.c43

Eckert, D.J. 1988. Soil pH. In: W.C. Dahnke, editor, Recommended chemical soil test procedures for the North Central Region. Bull. 221 (revised). North Dakota Agric. Exp. Stn., Fargo. p. 6–8.

Feng, W., C.P. Lin, R.J. Deschamps, and V.P. Drnevich. 1999. Theoretical model of a multisection time domain reflectometry measurement system. Water Resour. Res. 35:2321–2331.

Francisca, M., and M.A. Montoro. 2012. Measuring the dielectric properties of soil–organic mixtures using coaxial impedance dielectric reflectometry. J. Appl. Geophys. 80:101–109. doi:10.1016/j.jappgeo.2012.01.011

Geller, J.T., and J.R. Hunt. 1993. Mass transfer from nonaqueous phase organic liquid in water saturated porous media. Water Resour. Res. 29:833–835.

Giese, K., and R. Tiemann. 1975. Determination of the complex permittivity from thin-sample time domain reflectometry: Improved analysis of the step response waveform. Adv. Mol. Relax. Processes 7:45–59. doi:10.1016/0001-8716(75)80013-7

Haridy, S.A., M. Persson, and R. Berndtsson. 2004. Estimation of LNAPL saturation in fine sand using time-domain reflectometry. Hydrol. Sci. J. 49:987–1000. doi:10.1623/hysj.49.6.987.55729

Heimovaara, T., A. Focke, W. Bouten, and J. Verstraten. 1995. Assessing temporal variations in soil water composition with time domain reflectometry. Soil Sci. Soc. Am. J. 59:689–698. doi:10.2136/sssaj1995.03615995005900030009x

International Union of Pure and Applied Chemistry. 1997. Compendium of chemical terminology. Blackwell Scientific, Oxford, UK.

IUSS Working Group WRB. 2006. World reference base for soil resources 2006: A framework for international classification, correlation and communication. 2nd ed. World Soil Resour. Rep. 103. FAO, Rome.

Legates, D.R., and G.J. McCabe, Jr. 1999. Evaluating the use of "good-

ness-of-fit" measures in hydrologic and hydroclimatic model validation. Water Resour. Res. 35:233–241.

Mercer, J.W., and R.M. Cohen. 1990. A review of immiscible fluids in the subsurface: Properties, models, characterization, and remediation. J. Contam. Hydrol. 6:107–163. doi:10.1016/0169-7722(90)90043-G

Miller, J.J., and D. Curtin. 2007. Electrical conductivity and soluble ions. In: M.R. Carter and E.G. Gregorich, editors, Soil sampling and methods of analysis. 2nd ed. CRC Press, Boca Raton, FL. p. 161–171.

Mohamed, A.M.O. 2006. Principles and applications of time domain electrometry in geoenvironmental engineering. Dev. Arid Region Res. 5. CRC Press, Boca Raton, FL.

Mohamed, A.M.O., and R.A. Said. 2005. Detection of organic pollutants in sandy soils via TDR and eigendecomposition. J. Contam. Hydrol. 76:235–249. doi:10.1016/j.jconhyd.2004.09.002

Moroizumi, T., and Y. Sasaki. 2006. Estimating the nonaqueous-phase liquid content in saturated sandy soil using amplitude domain reflectometry. Soil Sci. Soc. Am. J. 72:1520–1526. doi:10.2136/sssaj2006.0212

Nadler, A., S. Dasberg, and I. Lapid. 1991. Timed domain reflectometry measurements of water content and electrical conductivity of layered soil columns. Soil Sci. Soc. Am. J. 55:938–943. doi:10.2136/sssaj1991.03615995005500040007x

Persson, M., and R. Berndtsson. 2002. Measuring nonaqueous phase liquid saturation in soil using time domain reflectometry. Water Resour. Res. 38(5). doi:10.1029/2001WR000523

Redman, J.D., and S.M. DeRyck. 1994. Monitoring non-aqueous phase liquids in the subsurface with multilevel time domain reflectometry probes. In: Proceedings of the Symposium on Time Domain Reflectometry in Environmental, Infrastructure, and Mining Applications, Evanston, IL. Spec. Publ. SP19-94. U.S. Bur. of Mines, Washington, DC.

Reusser, D.E., T. Blume, B. Schaefli, and E. Zehe. 2009. Analysing the temporal dynamics of model performance for hydrological models. Hydrol. Earth Syst. Sci. 13:999–1018. doi:10.5194/hess-13-999-2009

Rhoades, J.D., N.A. Manteghi, P.J. Shouse, and W.J. Alves. 1989. Soil electrical conductivity and soil salinity: New formulations and calibrations. Soil Sci. Soc. Am. J. 53:433–439. doi:10.2136/sssaj1989.03615995005300020020x

Rinaldi, V.A., and F.M. Francisca. 2006. Removal of immiscible contaminants from sandy soils monitored by means of dielectric measurements. J. Environ. Eng. 132:931–939. doi:10.1061/(ASCE)0733-9372(2006)132:8(931)

Robinson, D.A., and S.P. Friedman. 2002. The effective permittivity of dense packing of glass beads, quartz sand and their mixtures immersed in different dielectric backgrounds. J. Non-Cryst. Solids 305:261–267. doi:10.1016/S0022-3093(02)01099-2

Topp, G.C., J.L. Davis, and A.P. Annan. 1980. Electromagnetic determination of soil water content: Measurement in coaxial transmission lines. Water Resour. Res. 16:574–582. doi:10.1029/WR016i003p00574

Topp, G.C., J.L. Davis, and A.P. Annan. 1982. Electromagnetic determination of soil water content using TDR: I. Application to wetting fronts and steep gradients. Soil Sci. Soc. Am. J. 46:672–678. doi:10.2136/sssaj1982.03615995004600040002x

Yu, X., and X. Yu. 2006. Time domain reflectometry tests of multilayered soils. In: Proceedings of the 3rd International Symposium and Workshop on Time Domain Reflectometry for Innovative Geotechnical Applications, TDR 2006, West Lafayette, IN. 17–20 Sept. 2006. Paper no. 3.

Zhan, L.T., Q.Y. Mu, Y. Chen and R.P. Chen. 2013. Experimental study on applicability of using time-domain reflectometry to detect NAPLs contaminated sands. Sci. China Technol. Sci. 56:1534–1543. doi:10.1007/s11431-013-5211-8